AGU PUBLICATIONS

JGR

Journal of Geophysical Research: Earth Surface

RESEARCH ARTICLE
10.1002/2015JF003664

Key Points:
- Empirical shape parameters are defined to approximate the soil temperature
- The method is effective to reconstruct the soil temperature and the heat flux
- A calibrated set of parameters is proposed

Correspondence to:
M. Falocchi,
marco.falocchi@unibs.it

Citation:
Falocchi, M., S. Barontini, and R. Ranzi (2015), A parametrization of a steady periodic solution of the Fourier equation to model soil temperature dynamics, *J. Geophys. Res. Earth Surf.*, *120*, 1784–1802, doi:10.1002/2015JF003664.

Received 6 JUL 2015
Accepted 9 AUG 2015
Accepted article online 13 AUG 2015
Published online 9 SEP 2015

A parametrization of a steady periodic solution of the Fourier equation to model soil temperature dynamics

Marco Falocchi[1], Stefano Barontini[1], and Roberto Ranzi[1]

[1]Department of Civil, Environmental, Architectural Engineering and Mathematics, Università degli Studi di Brescia, Brescia, Italy

Abstract In dry days the temperature of the upper soil layers presents a characteristic asymmetric periodic-like pattern with a minimum in the morning and a maximum in the afternoon. In view of estimating the conductive heat component of the surface energy balance, at local, basin, and global scales, in this study we use a periodic series solution of the Fourier equation to develop a simple procedure to accurately reconstruct the soil temperature and heat flux profiles. The method is based on weighting and phasing the Fourier harmonics by means of coefficients which do not depend on the soil thermal properties but only depend on the shape of the temperature boundary condition. The proposed coefficients can be regarded to as site independent and with good approximation universal. In order to calibrate and test the procedure, measurements of soil temperature, soil heat flux, and soil water content, collected during the CividatEX Experiment (summer 2012, summer 2013, and spring and summer 2014), in Italy, were used. The method accurately reproduced the temperature observations at three measurement depths within the upper 20 cm soil layer. Once assessed the soil thermal conductivity, the method proved to be effective also in reproducing the measured soil heat flux. The procedure was furthermore validated reconstructing with good results the soil temperature dynamics measured by an independent micrometeorological station in a different environment.

1. Introduction

Soil thermal regime and heat budget play a key role in many natural processes in the upper soil layers. Indeed, the soil temperature interacts with the soil water dynamics, the soil fauna, and the chemical processes, thus affecting the soil ecosystems and pedogenesis and a number of surface phenomena such as fog formation and evapotranspiration.

Besides the temperature, the soil heat flux and the stored heat in the upper soil layers are important terms in the Earth surface energy balance [*Brutsaert*, 1982; *Wilson et al.*, 2002; *Ochsner et al.*, 2007; *Sauer et al.*, 2008] and they are required in many hydrometeorological models at the local [*Heusinkveld et al.*, 2004; *Barr et al.*, 2012], basin [*Ranzi et al.*, 2010; *Endrizzi et al.*, 2014], and global scales [*Liang et al.*, 1994; *Coughlan and Avissar*, 1996; *Kiehl and Trenberth*, 1997; *Murphy et al.*, 2009; *Trenberth et al.*, 2009; *Liu et al.*, 2014; *Wild et al.*, 2014]. Particularly, in recent years, studies regarding the closure of the near-surface energy balance at the local scale [*Heusinkveld et al.*, 2004; *Ochsner et al.*, 2007] pointed out that the magnitude of these contributions is usually comparable with that of the residuum of the energy balance [*Foken*, 2008].

The soil temperature dynamic has been thoroughly investigated both theoretically and experimentally. Classical studies modeled the soil heat conduction by solving the Fourier equation with various mathematical approaches, among which the Fourier analysis and the Laplace transform played an important role [*Carslaw and Jaeger*, 1959; *Crank*, 1979]. Later, other theoretical findings were proposed to solve the Fourier equation, e.g., in terms of fractional operators [*Wang and Bras*, 1999] or by means of the Green function [*Wang*, 2012], and a focus was made on the minimum number of soil temperature measurements to accurately reconstruct the soil thermal dynamics. As an example *Wang* [2012] based his analytical solution on a single depth measurement and *Huang et al.* [2014] analytically reconstructed the diurnal and annual cycles of the soil thermal field on the basis of two depth measurements. In case of long-lasting infiltration into the soil or evaporation from a bare soil, the heat flux is coupled with the water content flow [e.g., *Pilotti et al.*, 2002] and the purely diffusive Fourier equation is usually rewritten in terms of an advection-diffusion equation. After a formulation of the general problem stated by *Philip and De Vries* [1957], seminal solutions were developed in view

of investigating the effects of thermal gradients on the water content flow [*Philip*, 1957], and the contribution of water flow on the temperature dynamics in the soil [*Chudnovskii*, 1962]. Other analytical solutions of the advection-diffusion equation were proposed in terms of steady periodic functions and by means of the Laplace transform [*Gao et al.*, 2003]. Recently, the solution of the advection-diffusion equation was investigated focusing on the evaporation [*Gao et al.*, 2008] and on the infiltration [*Wang et al.*, 2012] as key processes of the hydrological cycle. In the case of long-lasting infiltration, *Wang et al.* [2012] investigated, on the basis of previous experimental and numerical studies [*Jaynes*, 1990], the effect of a constant water ponding on the soil thermal dynamics. Observing that the infiltration at the soil surface shows a periodic daily pattern, probably due to the thermally induced variation of the water viscosity, the Authors introduced higher-order harmonics to describe the thermal advective and diffusive processes in the soil.

Other experimental studies characterized the soil temperature regime under different land cover conditions [*Ballard*, 1972] and in case of climate unsteadiness. In this field, long-term data series were investigated to detect the effect of climate seasonality on the upper soil layers thermal dynamics, as a proxy to understand the biological response on the agricultural production [*Jacobs et al.*, 2011] (grassland in The Netherlands) and the evolution of forest communities [*Khydyakov and Reshotkin*, 2014] (forest-tundra zone in the Polar Urals). As an application in glacialized environment, *Taschner and Ranzi* [2002] monitored and studied the temperature dynamics of a debris covered glacier in order to validate the glacier temperature data collected by means of a remote sensing technique. Finally, the reconstruction of the vertical soil temperature profile, with in situ and laboratory measurements, allowed also to develop methods aiming at estimating the soil thermal properties (diffusivity, conductivity, and volumetric heat capacity) required to compute the soil heat flux and the soil heat storage [*Farouki*, 1981; *Evett et al.*, 2012; *Wang and Bou-Zeid*, 2012].

Even if current computational resources can provide detailed solutions in reasonable time, nowadays analytical solutions of the soil thermal dynamics are still used in current research as it is evidenced by the number of recent contributions. Analytical solutions in fact, besides enlightening physical phenomena, simplify, and reduce the computational effort of numerical methods and are used as test cases to validate numerical codes. Moreover, simple closed-form solutions are useful to parametrize large-scale models or energy budget models. As an example *Wang et al.* [2011] reported that the use of an analytical solution of the Fourier equation, in the framework of an urban canopy model, was even more effective at representing the thermal dynamics than a completely numerical scheme, and moreover, it avoided the computational errors of the numerical predictions.

In this paper, aiming at contributing to make more effective the use of analytical solutions to parametrize energy budget models, we provide a quick, general procedure to accurately reconstruct the temperature and heat flux dynamics at the soil boundary. The procedure is based on a site-independent parametrization of a classical periodic solution of the Fourier equation.

An initial attempt revealed that the upper soil temperature regimes at different depths were characterized by a daily periodicity superimposed to the annual periodicity. According to this scheme and assuming that the Fourier equation is linear, simple solutions are derived with the hypotheses of periodic boundary conditions, expressed in terms of trigonometric functions. Yet as it is observed particularly in dry days, the temperature of the upper soil layers is far from being described by only one trigonometric function. Indeed, the soil temperature signal is unsteady and asymmetric, as well as the air temperature one at the soil surface [e.g., *Ca'Zorzi and Dalla Fontana*, 1986]. Anyway, if the fluctuating component of the measured temperature is isolated, the decomposition in Fourier series applies and, assuming the soil as a homogeneous and semi-infinite domain, analytical solutions of the Fourier equation are derived in terms of trigonometric series [*Carslaw and Jaeger*, 1959; *van Wijk and De Vries*, 1963]. In order to do so, the boundary condition at the soil surface is decomposed in a trigonometric series of sine functions and the solution is obtained by means of the superposition principle. We adopted this series solution of the Fourier equation to interpret the soil temperature dynamics during dry days, and we parametrized the Fourier coefficients up to the third harmonic to effectively reconstruct the daily soil temperature at a certain depth.

In agreement to previous studies [*Wang*, 2012; *Wang and Bou-Zeid*, 2012], if the soil thermal properties are known and if the daily average temperature is uniform with depth, only one soil temperature data series, measured at one depth, is sufficient to reconstruct the subsurface temperature profiles. Otherwise, if the mean temperature is variable with depth, that is the most common condition, at least two series at different depths

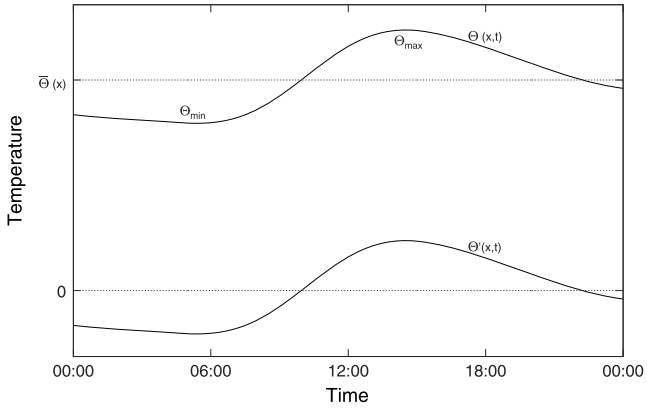

Figure 1. Sketch representing the components of the instantaneous temperature $\Theta(x,t)$ at a certain depth in the soil. According to equation (2), $\overline{\Theta}(x)$ and $\Theta'(x,t)$ are the daily time-average temperature and the fluctuation of the daily temperature cycle, respectively.

are required. From the subsurface temperature expressed in closed form, also the soil heat flux, the stored heat in a soil layer, and its ratio of change are easily derived.

In order to calibrate and validate the method, data of soil temperature at the depth of 5, 10, and 15 cm, of soil heat flux at 7.5 cm and of soil water content measured by a time domain reflectometry (TDR) probe at the depth of 5 cm were used. These data were collected during summer of 2012–2014 in the framework of the CividatEX Experiment (Cividate Camuno, 274 m above sea level (asl), Oglio river basin, Central Italian Alps) [*Negm et al.*, 2013; *Falocchi et al.*, 2015]. During the experiment a micrometeorological station was installed in a valley with complex topography to quantify the energy and water fluxes exchanged at the soil-atmosphere interface. After recalling the theoretical framework of the problem and presenting the developed procedure (section 2), the experimental site setup and the soil characteristics are described (section 3), finally the results are presented and discussed, and the procedure is tested with an application in a different environment (section 4).

2. Theory

2.1. Problem Statement and Stabilized Periodic Solution

The daily temperature dynamics of the upper soil layers can be modeled assuming the soil as a semi-infinite, a priori layered, domain where heat transfer can happen due to a number of phenomena as conduction, mass flow, and radiation [*van Wijk and De Vries*, 1963]. However, the problem can be progressively simplified, assuming that (i) the heat transfer is mainly vertical, (ii) the conduction is the main heat transfer process, (iii) the soil thermal properties are homogeneous in the upper soil layers, and (iv) heat sources and sinks are negligible. With these assumptions the soil heat transfer is fully described by the one-dimensional Fourier equation:

$$\frac{\partial \Theta}{\partial t} = \alpha \frac{\partial^2 \Theta}{\partial x^2}, \tag{1}$$

where $\Theta(x,t)$ is the instantaneous soil temperature, $\alpha[L^2T^{-1}]$ is the soil thermal diffusivity, which is homogeneous by hypothesis, t is the time variable, and x is the vertical coordinate, positive downward. The linearity of the Fourier equation allows us to apply the superposition principle to the problem and to obtain an analytical solution with a well-known theoretical framework as briefly summarized in the following lines. Assuming that the annual temperature fluctuation contribution to the instantaneous temperature profile is negligible at the daily scale, the temperature is rewritten as the sum of a constant term and of a fluctuating one, with null expectation, i.e.,

$$\Theta(x,t) = \overline{\Theta}(x) + \Theta'(x,t), \tag{2}$$

where $\overline{\Theta}(x)$ is the constant term represented by the daily time-average temperature and $\Theta'(x,t)$ is the fluctuating component. The last describes the daily temperature cycle, which at the soil surface typically shows a minimum in the early morning and a maximum presented in the sketch of Figure 1.

In order to provide a solution of (1) under Dirichlet boundary conditions we assume (as detailed in the Appendix A) that the daily temperature fluctuation $\Theta'(x,t)$ is a periodic function with a daily period and that the average temperature field $\overline{\Theta}(x)$ is either uniform or linear. A classical solution of the problem is taken in terms of stabilized periodic functions [*Chudnovskii*, 1962; *van Wijk and De Vries*, 1963]. This means that, considering a periodic boundary condition, after some time the solution does not depend anymore on the initial condition but only on the boundary conditions. Thus, the solution has the same periodicity of the upper boundary condition, and it is expressed as a Fourier series in the following form:

$$\Theta(x,t) = \overline{\Theta}(x) + \sum_{n=1}^{\infty} {}^{A}\Theta_{x,n} \sin\left(n\omega t + \phi_n(x)\right), \tag{3}$$

where $\overline{\Theta}(x)$ is the previously defined daily average soil temperature, ω is the daily radial, and ${}^{A}\Theta_{x,n} = {}^{A}\Theta_n(x)$ and $\phi_n(x)$ are the amplitude and the phase of each harmonic, respectively, at the depth x. The amplitude and the phase of the nth harmonic are related to the Fourier coefficients according to the relationships in the appendix ((A9) and (A10)). In the solution (3) the amplitudes contribute to approximate the maximum daily temperature excursion, and the phases allow us to adapt the pattern of the solution to the observed one. It can be proven that both these terms are depth dependent, according to:

$${}^{A}\Theta_{x,n} = {}^{A}\Theta_{o,n}\, e^{-\frac{x}{D_n}}, \tag{4}$$

$$\phi_n(x) = \phi_{o,n} - \frac{x}{D_n}, \tag{5}$$

where ${}^{A}\Theta_{o,n} = {}^{A}\Theta_n(0)$ is the surface amplitude, $\phi_{o,n} = \phi_n(0)$ is the phase at surface and D_n is the damping depth [L], all referred to the nth harmonic. The nth damping depth D_n is given by the relation:

$$D_n = \sqrt{\frac{2\alpha}{n\omega}}, \tag{6}$$

and it is therefore related to the soil diffusivity. Equation (4) allows to define the damping depth D_n as the depth at which the daily surface amplitude of the nth harmonic is reduced to its fraction e^{-1}, i.e., about 37%.

If the soil diffusivity α is not known and at least two soil temperature series at distinct depths are known, ${}^{A}\Theta_{o,n}$ and D_n can be easily estimated by fitting equation (4). Otherwise, if α is known, then only one temperature series is needed to estimate ${}^{A}\Theta_{o,n}$.

By means of the solution (3) and of the Fourier law, also the soil heat flux $H(x,t)$ and the stored soil heat (in a layer of a certain thickness) can be analytically computed. For the sake of brevity the procedure is reported in Appendix B.

2.2. Simplification of the Stabilized Periodic Solution

Let us define now the actual amplitude of the surface temperature ${}^{A}\Theta_o^*$ as follows:

$${}^{A}\Theta_o^* = \frac{1}{2}\left(\Theta_{\max} - \Theta_{\min}\right), \tag{7}$$

where $\Theta_{\max}$ and $\Theta_{\min}$ are the maximum and the minimum daily temperature, respectively. Let us also define the coefficient $\epsilon_{A,n}$:

$$\epsilon_{A,n} = \frac{{}^{A}\Theta_{o,n}}{{}^{A}\Theta_o^*}, \tag{8}$$

as the ratio between the nth surface amplitude ${}^{A}\Theta_{o,n}$ and the actual surface amplitude ${}^{A}\Theta_o^*$. Based on the observation that during dry days the fluctuation of the measured soil temperature has a constant periodic pattern, similar at different depths, we introduce the hypothesis that the ratio $\epsilon_{A,n}$ and the nth phase $\phi_n(x)$ are constant.

Being the damping of the nth harmonic described by (4), we assume that also the damping of the actual amplitude ${}^{A}\Theta^*(x)$ is described by means of an exponential function:

$${}^{A}\Theta^*(x) = {}^{A}\Theta_o^*\, e^{-\frac{x}{D^*}}, \tag{9}$$

where D^* is the bulk damping depth. As for (4) if at least two temperature series at two different depths are available, ${}^A\Theta_o^*$ and D^* can be estimated after (9), for instance, with a best fit. Analogously to (6) we assume that also the bulk damping depth D^* is related to the soil diffusivity α and to the daily radial frequency ω, as

$$D^* \propto \sqrt{\frac{2\alpha}{\omega}}. \tag{10}$$

If (10) holds, also the ratio

$$\epsilon_{D,n} = \frac{D^*}{D_n}, \tag{11}$$

between the bulk damping depth D^* and the nth damping depth D_n is constant. This conclusion is supported by the experimental evidence, as we will show in the followings. By virtue of the assumption (10), $\epsilon_{D,n}$ does not depend on the soil thermal properties. Substituting (8) and (11) into equation (4) we obtain the following expression for ${}^A\Theta_{x,n}$:

$${}^A\Theta_{x,n} = \epsilon_{A,n}\,{}^A\Theta_o^*\, e^{-\epsilon_{D,n}\frac{x}{D^*}}. \tag{12}$$

Equation (12) points out the physical meaning of the coefficients $\epsilon_{A,n}$ and $\epsilon_{D,n}$. In fact, $\epsilon_{A,n}$ describes how smaller the surface amplitude of the nth harmonic is than the actual one ${}^A\Theta_o^*$, and $\epsilon_{D,n}$ describes how faster the amplitude of the nth harmonic decays than the actual amplitude ${}^A\Theta^*(x)$ does.

If the surface phase $\phi_{o,n}$ is determined from (5) then the following nth set of coefficients $\mathcal{F}_n$:

$$\mathcal{F}_n = \left(\phi_{o,n},\, \epsilon_{A,n},\, \epsilon_{D,n}\right), \tag{13}$$

does not depend on the soil thermal properties, nor on the depth x, not on the amplitude of the daily temperature fluctuation, but only on the pattern and on the phase of the daily temperature cycle.

The coefficients $\epsilon_{A,n}$ and $\epsilon_{D,n}$ are properties of the pattern of the surface temperature, and they can be regarded to as site independent. The phases $\phi_{o,n}$ refer instead to the conventional local time and can depend on local geomorphological and climate conditions. As a first approximation and disregarding any local effects, a generalized value $\phi_{o,n}^*$ referred to the real local time is obtained as

$$\phi_{o,n}^* = \phi_{o,n} - \Delta\lambda. \tag{14}$$

In (14) $\Delta\lambda$, expressed in radians, is the difference $\Delta\lambda = \lambda_s - \lambda_m$, between the longitude of the experimental site λ_s and that of the reference meridian of the time zone λ_m.

We therefore propose to simplify the analytical solution (3) by substituting into each harmonic the set of coefficients $\mathcal{F}_n$ (13). Defining N the highest considered order of harmonics, the equation for the fluctuating component is simplified and approximated as

$$\Theta'(x,t) \approx \sum_{n=1}^{N} \epsilon_{A,n}\,{}^A\Theta_o^*\, e^{-\epsilon_{D,n}\frac{x}{D^*}} \sin\left(n\omega t + \phi_{o,n} - \epsilon_{D,n}\frac{x}{D^*}\right). \tag{15}$$

The contribution, given to the heat flux (B2) by the temperature fluctuation, is estimated by means of the partial derivative,

$$\frac{\partial\Theta'}{\partial x} \approx -\sqrt{2}\sum_{n=1}^{N} \epsilon_{A,n}\epsilon_{D,n}\frac{{}^A\Theta_o^*}{D^*} e^{-\epsilon_{D,n}\frac{x}{D^*}} \sin\left(n\omega t + \phi_{o,n} - \epsilon_{D,n}\frac{x}{D^*} + \frac{\pi}{4}\right), \tag{16}$$

and, if calculated at the soil surface, by

$$\left.\frac{\partial\Theta'}{\partial x}\right|_{x=0} \approx -\sqrt{2}\sum_{n=1}^{N} \epsilon_{A,n}\epsilon_{D,n}\frac{{}^A\Theta_o^*}{D^*} \sin\left(n\omega t + \phi_{o,n} + \frac{\pi}{4}\right). \tag{17}$$

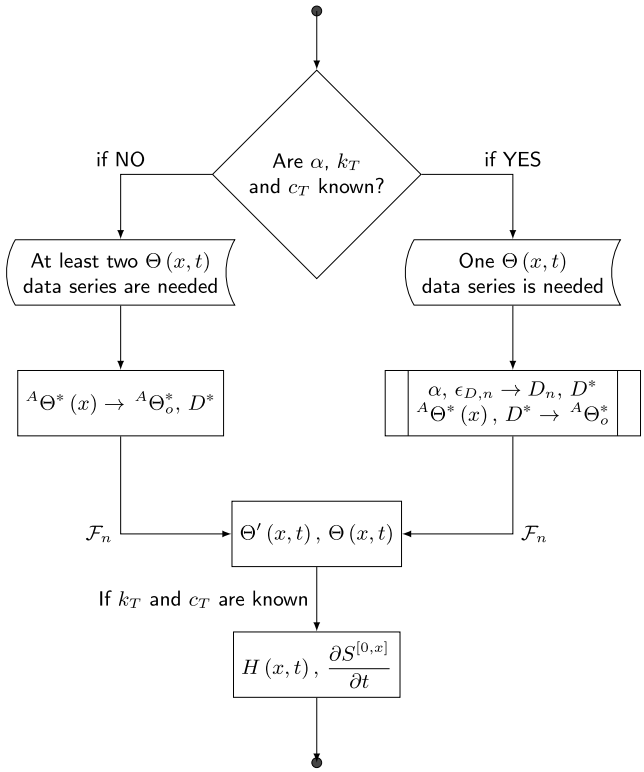

Figure 2. Stepwise diagram of the procedure presented in section 2.3.

Therefore, equations (B3) and (B4), respectively, become

$$H(x,t) = -k_T \left[\frac{\partial \overline{\Theta}}{\partial x} - \sqrt{2} \sum_{n=1}^{N} \epsilon_{A,n} \epsilon_{D,n} \frac{{}^{A}\Theta^{*}_{o}}{D^{*}} \mathrm{e}^{-\epsilon_{D,n} \frac{x}{D^{*}}} \sin\left(n\omega t + \phi_{o,n} - \epsilon_{D,n} \frac{x}{D^{*}} + \frac{\pi}{4} \right) \right], \tag{18}$$

$$H(0,t) = -k_T \left[\frac{\partial \overline{\Theta}}{\partial x} - \sqrt{2} \sum_{n=1}^{N} \epsilon_{A,n} \epsilon_{D,n} \frac{{}^{A}\Theta^{*}_{o}}{D^{*}} \sin\left(n\omega t + \phi_{o,n} + \frac{\pi}{4} \right) \right]. \tag{19}$$

According to (B8) the rate of change of the heat stored in the layer above x is given by

$$\frac{\partial S^{[0,x]}}{\partial t} = c_T \int_0^x \frac{\partial \Theta'}{\partial t} \mathrm{d}\xi \approx c_T \frac{\omega}{\sqrt{2}} \sum_{n=1}^{N} n \frac{\epsilon_{A,n}}{\epsilon_{D,n}} D^{*}\, {}^{A}\Theta^{*}_{o} \left[\sin\left(n\omega t + \phi_{o,n} + \frac{\pi}{4} \right) - \mathrm{e}^{-\epsilon_{D,n} \frac{x}{D^{*}}} \sin\left(n\omega t + \phi_{o,n} - \epsilon_{D,n} \frac{x}{D^{*}} + \frac{\pi}{4} \right) \right]. \tag{20}$$

As it is reported in the literature [e.g., *van Wijk and De Vries*, 1963; *Ballard*, 1972], the typical asymmetric periodic-like pattern of the soil temperature is well approximated by the first three harmonics. The higher-order harmonics contribute to describe the daily unsteadiness and they are daily sensitive. Accordingly, in order to focus on the daily temperature pattern, we chose $N = 3$ as the highest-order harmonic and, in section 3.3 and Table 2, we propose the set of coefficients $\mathcal{F}_n$ estimated after equations (4), (5), (8), (9), and (11). The coefficients $\mathcal{F}_n$ are obtained on the basis of data collected during the experimental field campaign presented in section 3.1.

2.3. How to Use the $\mathcal{F}_n$ Coefficients

The $\mathcal{F}_n$ coefficients are theoretically independent on the soil thermal properties and are only function of the pattern of the soil temperature series. As soon as the temperature profiles can be decomposed as in (2) and the fluctuating component has the typical dry day's shape, the coefficients $\mathcal{F}_n$ can be regarded to as universal. In this case in order to accurately reconstruct all the temperature profiles, the heat flux, and the heat stored in a finite soil layer, the following quick procedure applies (see Figure 2 for a schematic resume).

Table 1. Soil Porosity ϕ, Bulk Density ρ_b, Grain Size Distribution Percentages, and Correspondent USDA Textural Class, for the Investigated Soil Layers

Layer	Depth (cm)	ϕ (–)	ρ_b (g cm^{-3})	Gravel (%)	Sand (%)	Silt (%)	Clay (%)	USDA Textural Class
A	0–9	0.53	1.24	44.64	14.70	29.71	10.96	Silty loam
C1	9–22	0.44	1.49	44.59	15.73	27.77	11.91	Loam
C2	22–38	0.50	1.32	59.22	12.11	20.92	7.75	Silty clay loam
D	> 38	–	–	88.57	2.33	7.13	1.97	Silty loam

Given at least two series of soil temperature measurements at distinct depths and if the soil thermal conductivity is either known or estimated through empirical relationships (see for a review *Farouki*, [1981]), then (1) the profile of the daily average soil temperatures is interpolated by means of (A2); (2) the fluctuating component of the temperature series is day by day separated by means of (2); (3) the surface actual amplitude ${}^{A}\Theta_o^*$ and the bulk damping depth D^*, for each day, are obtained fitting (9); (4) the local phase coefficients $\phi_{o,n}$ are determined by means of (14); (5) the temperature fluctuations $\Theta'(x,t)$ are given by (15) with the coefficients reported in Table 2; (6) according to (2), the temperature profiles $\Theta(x,t)$ are reconstructed by means of (15) and (A2); (7) the heat flux profiles $H(x,t)$ are determined by means of the Fourier law rewritten as (18) or (19); (8) the bulk damping depth D^* and the coefficients $\epsilon_{D,n}$ of Table 2 allow to determine both D_n, by means of (11), and a representative value of the soil diffusivity α after (6); (9) the heat capacity c_T is then estimated by means of (B6); (10) finally, the rate of change of the heat stored in the uppermost soil layer is given by (20).

If only one series of soil temperature measurements is available, the procedure still applies, but reliable estimates of at least two soil thermal properties are required. In this case in fact items 8 and 9 of the procedure allow to determine D^*. Afterward, items 1–3 allow to determine ${}^{A}\Theta_o^*$, thus providing the required parameters for items 5–7 and 10.

3. Case Study

3.1. Field Campaign

During summer 2012, summer 2013 and spring and summer 2014 the CividatEX Experiment [*Negm et al.*, 2013; *Falocchi et al.*, 2015] was performed at Cividate Camuno (274 m asl, Oglio river basin, Central Italian Alps), aiming at assessing the energy and water balance at the local scale in a mountain environment, characterized by a typical Alpine sublitoranean climate [*Bandini*, 1931]. The experimental site is a flat gentle sloping lawn, at the feet of a hill, on an ancient alluvial shelf. The lawn is mainly covered by common grass between which short-spontaneous vegetation grows, mainly, alfalfa (*Medicago sativa*), wild carrot (*Daucus carota*), and yarrow (*Achillea millefolium*), which can reach a height of about 0.6 m at maturation. The soil under the lawn is a shallow and nonmature Technosol, characterized by three horizons: A (0 to 9 cm), C (9 to 38 cm), and D (below 38 cm). The layer C evidenced two subhorizons, which were defined C1 and C2, due to the different presence of roots and to the different skeletal fraction. Laboratory tests to determine the grain size distribution curve and to assess soil hydrological properties were performed. For a more complete description of the experimental site and the soil physical properties, please refer to *Negm et al.* [2013] and *Falocchi et al.* [2015]. In Table 1 the porosity, the bulk density, and the grain size distribution obtained per each layer with the corresponding U.S. Department of Agriculture (USDA) soil texture [*U.S. Department of Agriculture*, 1999] are reported. The soil temperature measurements were collected within layers A and C.

Among the measured micrometeorological variables, the following ones were of interest for this study: the soil temperature at the depths of 5, 10, and 15 cm measured with three thermocouples; the heat flux measured at the depth of 7.5 cm with a LSI-LASTEM heat fluxmeter (summer 2012) and a Hukseflux HFP01 fluxmeter (spring and summer 2014); and the soil water content at the depth of 5, 15, 22, and 37.5 cm measured with four TDR multiplexed probes. The thermocouples and the soil fluxmeters sampled every minute and the TDR apparatus every 5 min.

For this study 43 dry days were selected from 17 July to 26 September 2012 to estimate representative values for the set (13) with $n = 1, 2$, and 3, and 11 dry days selected from 21 June to 9 July 2013, and 10 consecutive (but not all dry) days from 1 to 10 June 2014 were used to validate the procedure. The soil thermal conductivity was calibrated on the basis of 37 dry days collected in summer 2012 and from 53 dry days collected in spring and summer 2014.

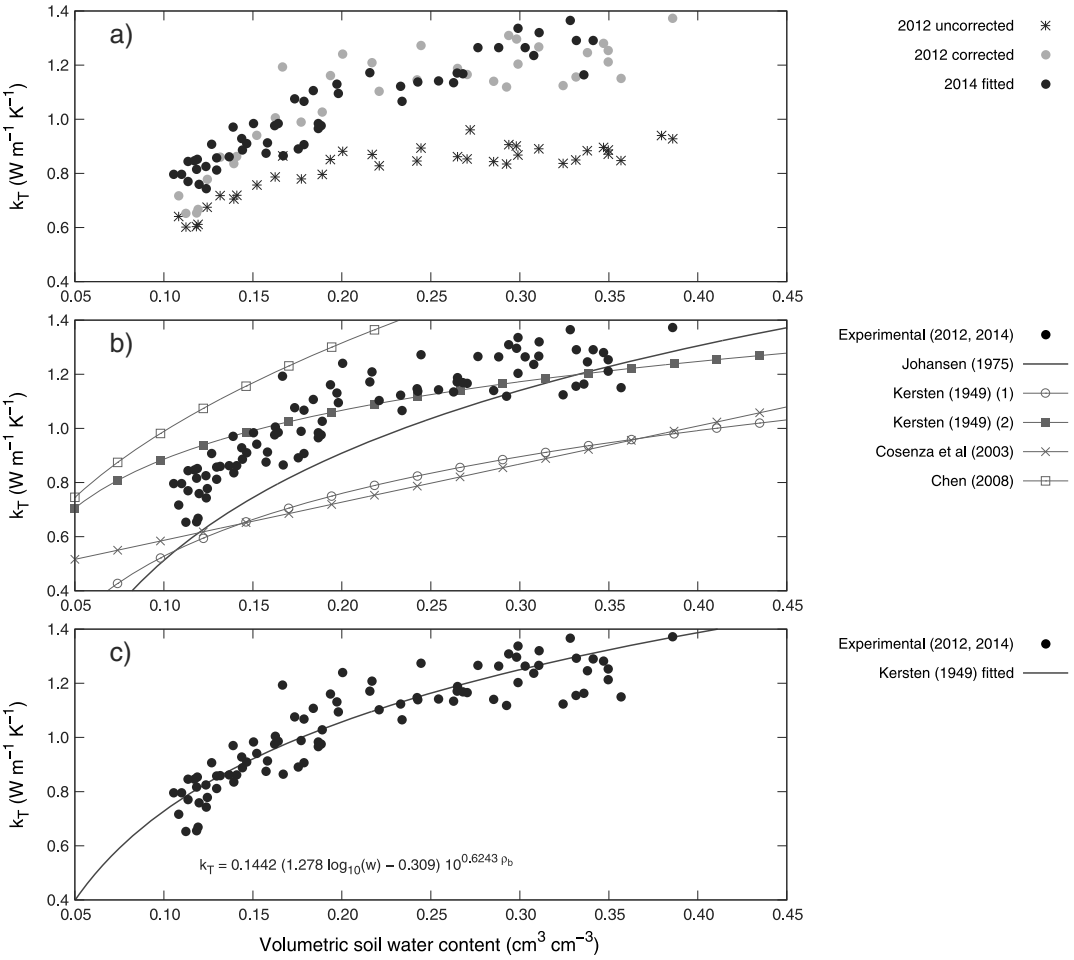

Figure 3. Soil thermal conductivity k_T versus the daily average volumetric soil water content. (a) Effect of the correction of the heat fluxes proposed by *Philip* [1961] on the estimate of k_T. (b) Experimental values of k_T (points) and literature models of k_T functions for a fine natural unfrozen soil with a quartz content of 53% [*Johansen*, 1975]; an unfrozen fine soil with silt-clay content greater than 50% (1) and an unfrozen coarse soil (2) [*Kersten*, 1949]; a sandy clay loam, after a numerical solution [*Cosenza et al.*, 2003]; and a sand [*Chen*, 2008]; (c) Experimental values of k_T (points) and fitted empirical relationship on the basis of Kersten's model.

3.2. Estimate of the Soil Thermal Properties

The soil thermal properties k_T, c_T, and α are a function of the thermal properties of the soil components and are sensitive to the water content. When no rainfall occurs and particularly during dry days, the soil water dynamics are slow, if compared to the temperature ones. As a first attempt, the soil thermal properties can be considered constant during the day and put into relation with the average soil water content. Therefore, we determined a daily value of the soil thermal conductivity $k_T(w)$, depending on the daily average gravimetric soil water content w, as a fitting parameter of the Fourier law (B1). The thermal gradient $\frac{\partial \Theta}{\partial x}$ was estimated

Table 2. The Weighting Factors of the Amplitude $\epsilon_{A,n}$, the Damping Depth $\epsilon_{D,n}$, the Surface Phase $\phi_{o,n}$ and the Generalized Phase $\phi^*_{o,n}$ With Their Correspondent Average μ, Standard Deviation σ, and Standard Error s_e up to the Third Harmonic

		$n=1$			$n=2$			$n=3$		
		μ	σ	s_e	μ	σ	s_e	μ	σ	s_e
$\epsilon_{A,n}$	(-)	0.910	0.081	0.012	0.212	0.061	0.009	0.053	0.035	0.005
$\epsilon_{D,n}$	(-)	0.958	0.109	0.017	1.245	0.238	0.036	1.047	0.730	0.111
$\phi_{o,n}$	(rad)	3.825	0.113	0.018	0.639	0.275	0.045	4.702	0.935	0.152
$\phi^*_{o,n}$	(rad)	3.908			0.722			4.785		

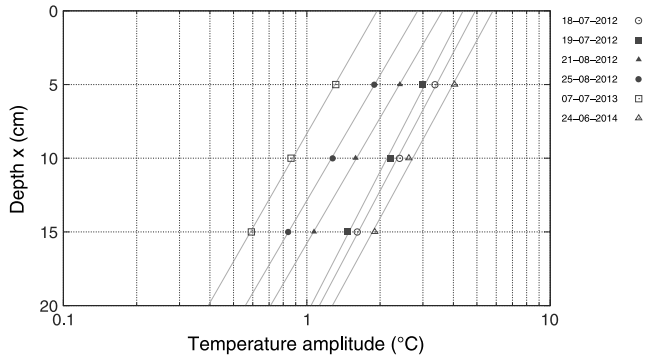

Figure 4. Verification of the assumption (9) about the exponential decay of the actual amplitude ${}^{A}\Theta^{*}(x)$ of the soil temperature signals with depth. As an example actual amplitudes measured during 6 days are represented.

after (3) at the depth of the measured heat flux, i.e., 7.5 cm. In order to investigate the dependence of $k_T(w)$ on the soil water content w, data collected by the TDR probe at 5 cm were considered. Once known the damping depth D_n for each harmonic, a representative value of the thermal diffusivity α was determined after (6). As D_n and α are calculated on a daily basis, they indirectly account for the current soil water content. Then the heat capacity $c_T(w)$ was determined after (B6). When traditional fluxmeters are used, the measured soil heat flux is usually underestimated [*Sauer and Horton*, 2005], mainly due to (i) the poor contact between the fluxmeter and the soil especially if the soil is coarse [*Weber et al.*, 2007], (ii) the modification induced by the shape of the device to the heat flow field, and (iii) the different thermal conductivity between the device and the surrounding soil, that is more evident when the soil is wet [*Mogensen*, 1970]. According to *Philip* [1961] reliable estimates of the actual flux H are obtained if the measured flux H', provided by a circular fluxmeter, is corrected by means of the coefficient c:

$$c = \frac{H'}{H} = \frac{1}{1 - 1.74\,\frac{d}{\sqrt{A}}\left(1 - \frac{k_T}{k_T'}\right)}, \tag{21}$$

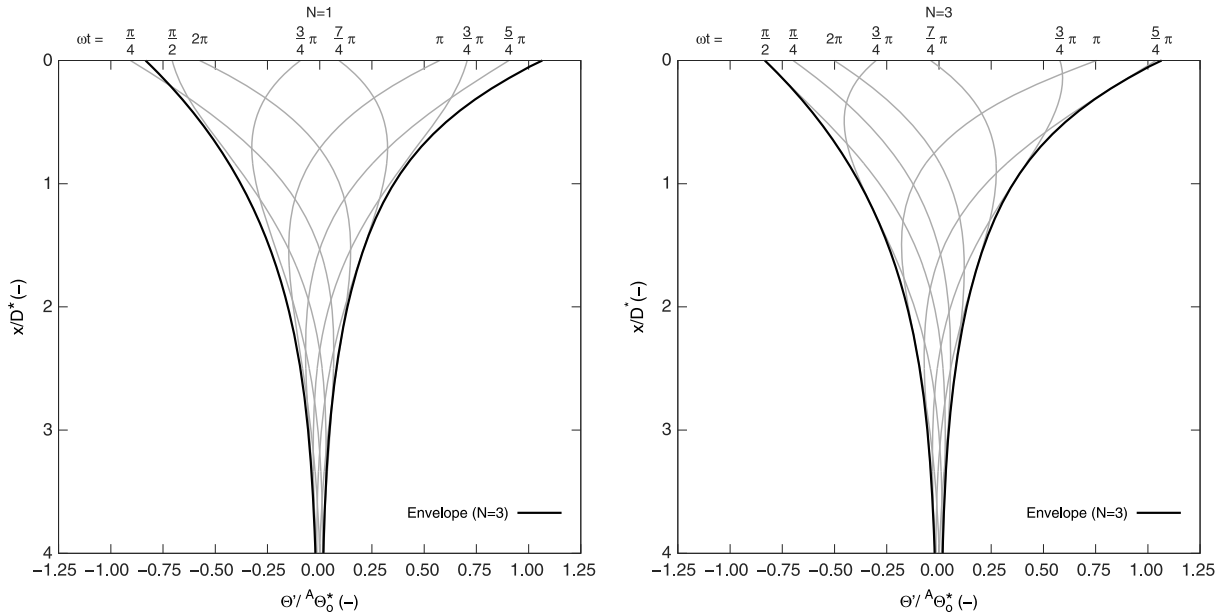

Figure 5. Dimensionless profiles of the fluctuating component of the temperature obtained with the simplified (15) for (left) $N = 1$ and (right) $N = 3$ harmonics. The envelope of the profiles for $N = 3$ harmonics is represented in both the graphs, in order to emphasize the asymmetry introduced by the second and third harmonics. The phases $\phi_{o,n}$ are referred to the conventional local time. As $\phi_{o,1} = 3.825$ rad, the minimum and maximum surface values for $N = 1$ are close to those obtained for $\omega t = \frac{\pi}{4}$ and $\frac{5}{4}\pi$, respectively.

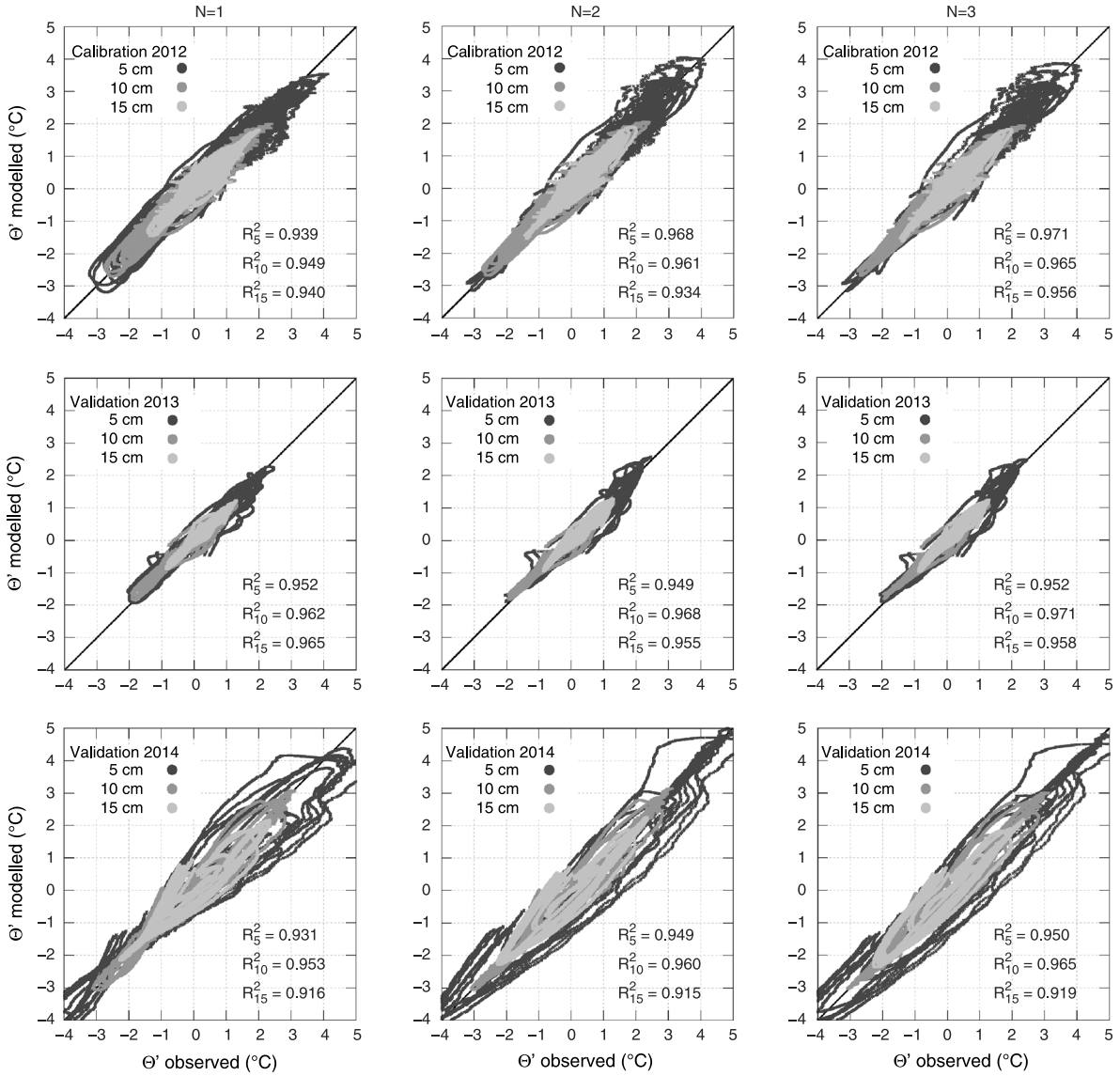

Figure 6. Scatterplot of observed and modeled temperature fluctuations at each depth, at increasing the number of harmonics *N*, for (top row) the calibration and (middle and bottom rows) the validation periods. Dry days were selected for 2012 and 2013 and 10 consecutive but not all dry days were selected in 2014.

where d is the thickness of the fluxmeter, A is its cross section, $k_T(w)$ is the (unknown) thermal conductivity of the soil, and k'_T is that of the sensor. This correction mainly accounts for the heat field distortion and during our work was applied to data collected in 2012 as the fluxmeter was thick and with a small diameter. Accounting for the Fourier law (B1), c is also equal to

$$c = \frac{k'_T}{k_T}. \tag{22}$$

Equations (21) and (22) therefore allow to determine c and k_T each day. In Figure 3a the conductivity data of 2012 and 2014 are reported. It is observed that values of k_T for year 2012 determined on the basis of uncorrected fluxes are meaningfully smaller than those determined on the basis of corrected fluxes. The latter are in good agreement with those determined on the basis of 2014 data.

In view of determining an analytical form of the thermal conductivity function $k_T(w)$, literature models used for soils with a relatively close taxonomy to that of the investigated one were considered. In Figure 3b it is observed that the experimental points are intercepted by Kersten's model (*Kersten* [1949] for an unfrozen coarse soil), and they are bounded by Johansen's model (*Johansen* [1975] for an unfrozen fine soil with a

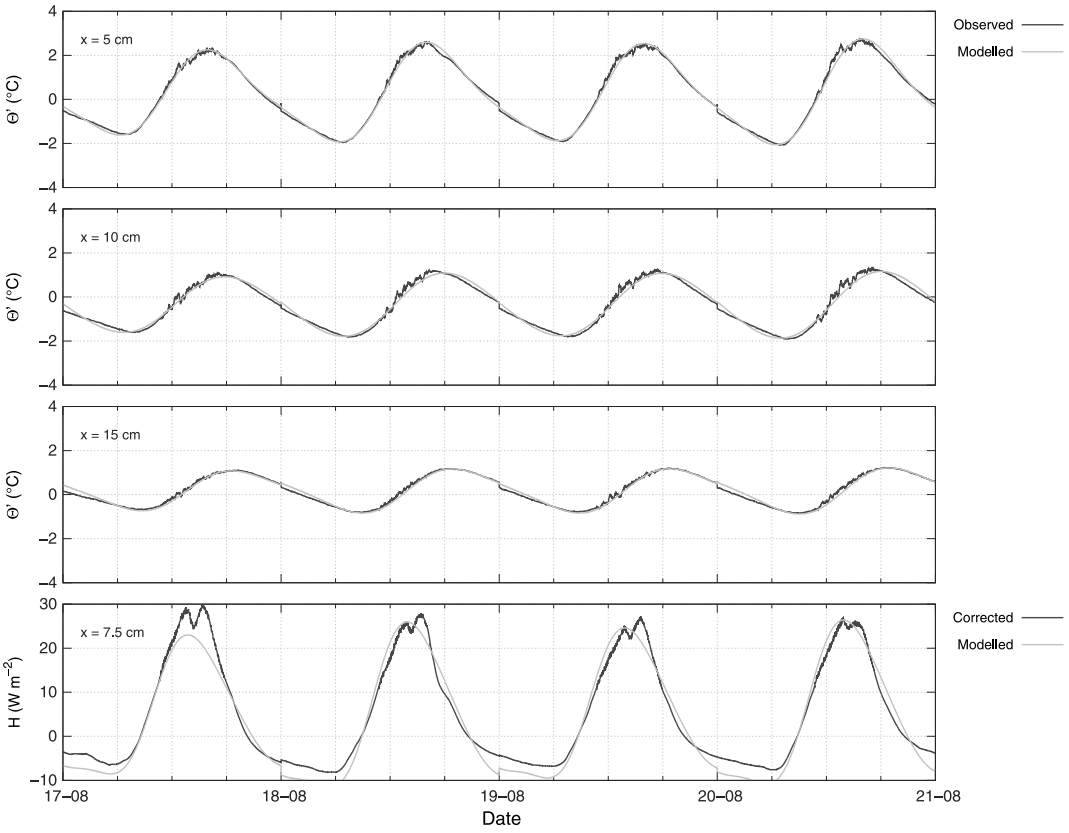

Figure 7. Observed and reconstructed soil temperature fluctuations at 5, 10, and 15 cm and soil heat flux at 7.5 cm, during four consecutive days of clear-sky conditions (August 2012, calibration period). Data collected during the CividatEX Experiment.

quartz content of 53%) and by Chen's model (*Chen*, [2008] for a sand), but none of the literature models fits the data. Therefore, an empirical $k_T(w)$ function was fitted (Figure 3c) on the basis of Kersten's model in the form:

$$k_T = 0.1442 \left(a \log_{10}(w) + b\right) 10^{0.6243\rho_b}, \tag{23}$$

where $a = 1.278$, $b = -0.309$, ρ_b is in g cm^{-3}, and k_T is in W m^{-1}K^{-1}.

3.3. Calibration of the $\mathcal{F}_n$ Coefficients

The soil temperature data measured at the three depths of 5,10, and 15 cm were filtered by means of a centered moving average of 15 min window, in order to reduce the high-frequency noise of the signal. Then the daily averages ($\overline{\Theta}_5$, $\overline{\Theta}_{10}$, $\overline{\Theta}_{15}$) and the actual amplitudes ($^A\Theta^*_5$, $^A\Theta^*_{10}$, $^A\Theta^*_{15}$) were computed and fitted against depth. The averages were well interpolated by a linear trend and the coefficients of (A2) were fitted. The actual amplitudes were interpolated according to (9), thus estimating the actual amplitude of the thermal wave at surface $^A\Theta^*_o$ and the bulk soil damping depth D^*.

The fluctuating component $\Theta'(x,t)$ was obtained by means of (2), substituting the interpolated daily average $\overline{\Theta}(x)$. Then the Fourier coefficients $a_{x,n}$ and $b_{x,n}$, defined in (A4) and (A5), were approximated (for each day) by means of the relationships:

$$a_{x,n} \cong \frac{2}{p} \sum_{j=1}^{p} \Theta'\left(x, t_j\right) \cos\left(2\pi n \frac{j}{p}\right), \tag{24}$$

$$b_{x,n} \cong \frac{2}{p} \sum_{j=1}^{p} \Theta'\left(x, t_j\right) \sin\left(2\pi n \frac{j}{p}\right), \tag{25}$$

and they were computed up to the third-order harmonic at each measuring point. In equations (24) and (25) p is the number of available data per day. The relationships (A9) and (A10) allowed to estimate for the nth

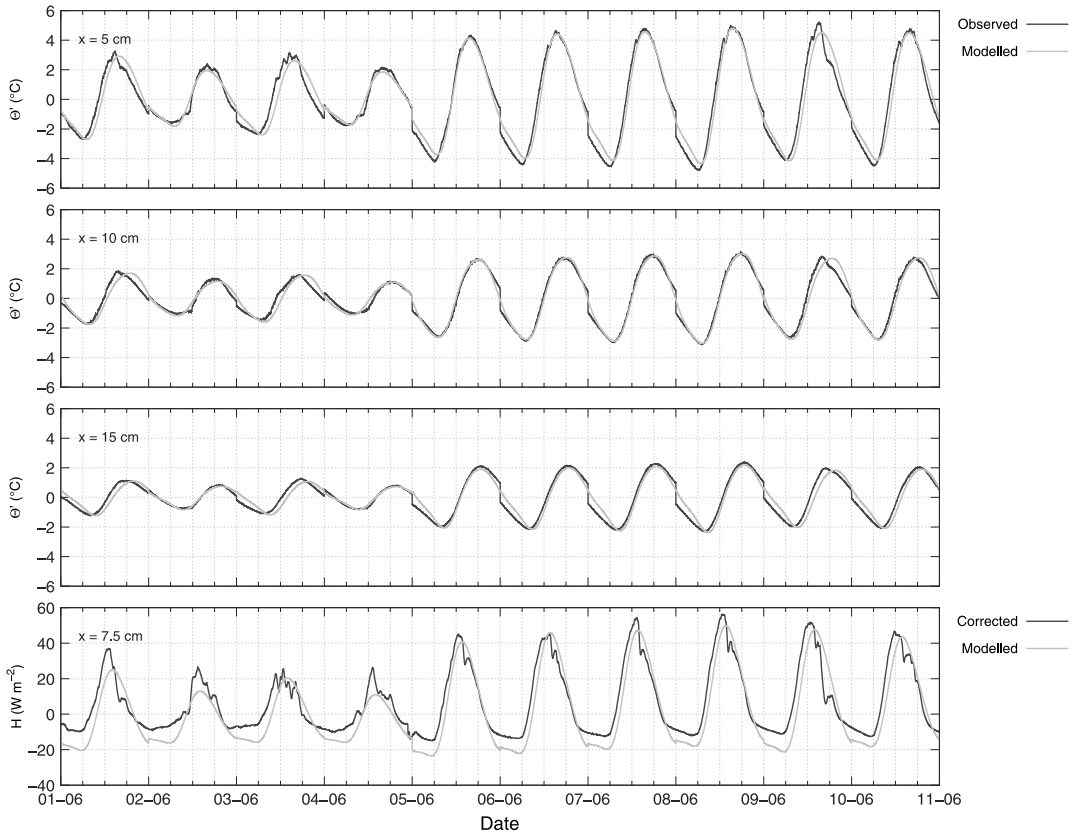

Figure 8. Observed and reconstructed soil temperature fluctuations at 5, 10, and 15 cm and soil heat flux at 7.5 cm, during 10 consecutive days (June 2014, validation period). Data collected during the CividatEX Experiment.

harmonic the corresponding amplitude ${}^{A}\Theta_{x,n}$ and phase $\phi_{x,n}$. By means of (4) and (5), also the surface amplitudes ${}^{A}\Theta_{o,n}$, the damping depth D_n, and the phase at surface $\phi_{o,n}$ were computed. This procedure allowed to determine for each *i*th day the set of coefficients $\mathcal{F}_{n,i}$ expressed by (13). Then also the daily diffusivity α was computed by means of (6), as an average of the diffusivities estimated for each harmonic.

A representative value of the set $\mathcal{F}_n$ was obtained by averaging the daily values of each term. The estimates $\epsilon_{A,n}$, $\epsilon_{D,n}$, $\phi_{o,n}$, defined as

$$\epsilon_{A,n} = \frac{1}{M}\sum_{i=1}^{M}\frac{{}^{A}\Theta_{o,n,i}}{{}^{A}\Theta^{*}_{o,i}}, \tag{26}$$

$$\epsilon_{D,n} = \frac{1}{M}\sum_{i=1}^{M}\frac{D^{*}_{i}}{D_{n,i}}, \tag{27}$$

$$\phi_{o,n} = \frac{1}{M}\sum_{i=1}^{M}\phi'_{o,n,i}, \tag{28}$$

where M is the number of the selected days to determine $\mathcal{F}_n$, are reported in Table 2 for the first three harmonics.

4. Results and Discussion

Once verified, the assumption (9) regarding the exponential decay of the actual amplitude (Figure 4), the weighting factors of the amplitude $\epsilon_{A,n}$, and of the damping depth $\epsilon_{D,n}$, and the average surface phase $\phi_{o,n}$, were determined according to (26) – (28) up to the third harmonic, using 43 dry days in 2012. The estimates are reported in Table 2 together with their standard deviations σ and the standard errors $s_e = \sigma/\sqrt{M}$, where M is the number of samples. The coefficients reported in Table 2 indicate that the amplitude of the daily fluctuation

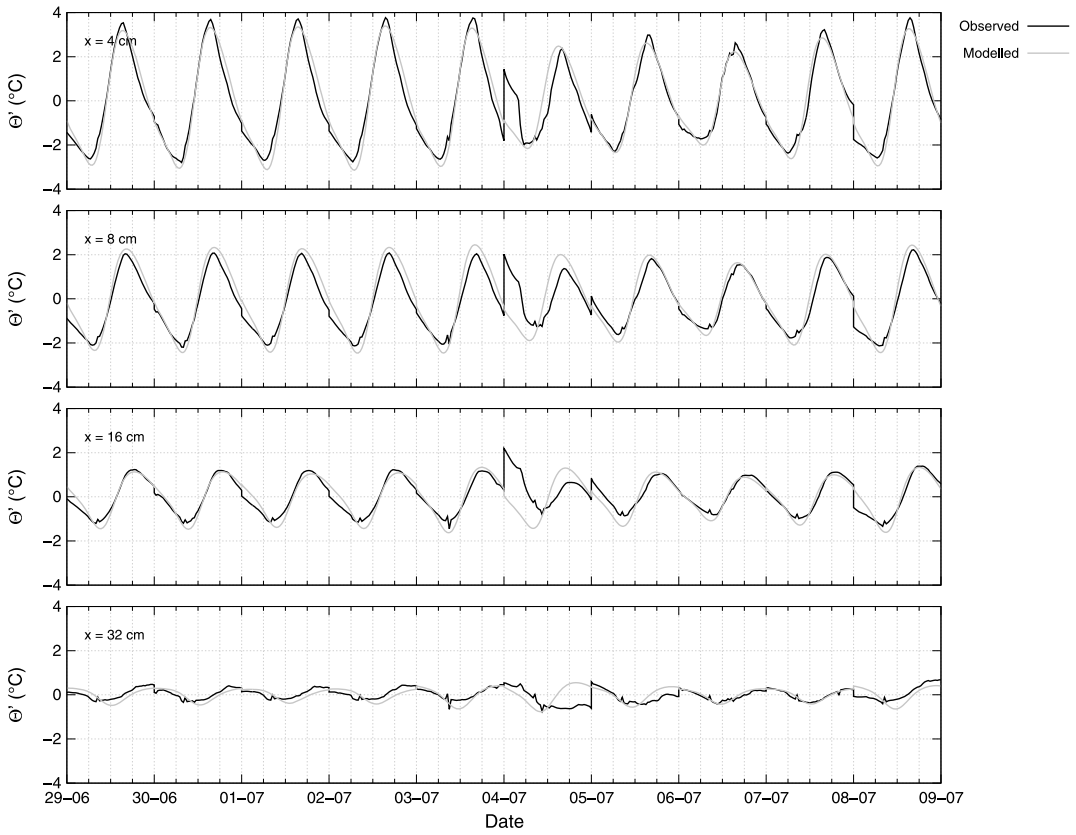

Figure 9. Observed and reconstructed soil temperature fluctuations at the depths of 4, 8, 16, and 32 cm, during 10 consecutive days (June and July 1997, model application). Data collected by the NOAA/ATDD micrometeorological station at Chickasha (Little Washita watershed, Oklahoma, USA) [*Meyers*, 2015].

is mainly represented by the first-order harmonic. However, higher-order harmonics describe the asymmetry of the series [see, e.g., *van Wijk and De Vries*, 1963]. As an example the corresponding profiles of the fluctuating component Θ' by means of equation (15) are represented in dimensionless form in Figure 5, both for a solution with one harmonic only and for the solution with three harmonics. The envelope of the profiles represented in both the graphs for $N = 3$ harmonics evidences the role played by the second and third harmonics at breaking the symmetry of the temperature series. In Figure 6 the observed and modeled temperature fluctuations (at 5, 10, and 15 cm) are scattered both for the calibration (2012) and for the validation period (2013 and 2014). The comparisons were performed separately per each depth and at increasing the number N of harmonics in (15). The asymmetry of the temperature series is more evident just below the soil surface and for a thickness of few centimeters, indeed the upper soil layer temperature (at 5 cm depth) is more asymmetric than the two deeper signals. This is due to the effect of the soil diffusivity which behaves as a low-pass filter and progressively damps the thermal waves with smaller period than the daily cycle. This observation is in agreement with the fact that the damping depths of the second and third harmonics, expressed in terms of weighting coefficient $\epsilon_{D,n}$ introduced by equation (11), are smaller than that of the first one. The obtained results show a good agreement, between the model and the observations, at reconstructing both the maximum, the minimum, and the asymmetry of the signals. Comparing the scatterplot of the two validation periods some differences emerge. At first the temperature fluctuations in the selected days of 2013 were smaller than those of the selected days of 2014. Then the modeled data are more dispersed around the best agreement line in 2014 than in 2013. The greater dispersion and greater fluctuations should be related to the fact that 2014 days were chosen in late spring (1 to 10 June) and 2012 and 2013 days were chosen during summer (July and August). Due to the local geomorphological configuration, a slightly different phase is observed in the temperature signal between late spring and summer, thus resulting in a greater dispersion around the agreement line. Moreover, for a further validation of the model in 2014 both dry and rainy days were chosen. Rainy days show a less regular temperature pattern which contribute to increase the dispersion.

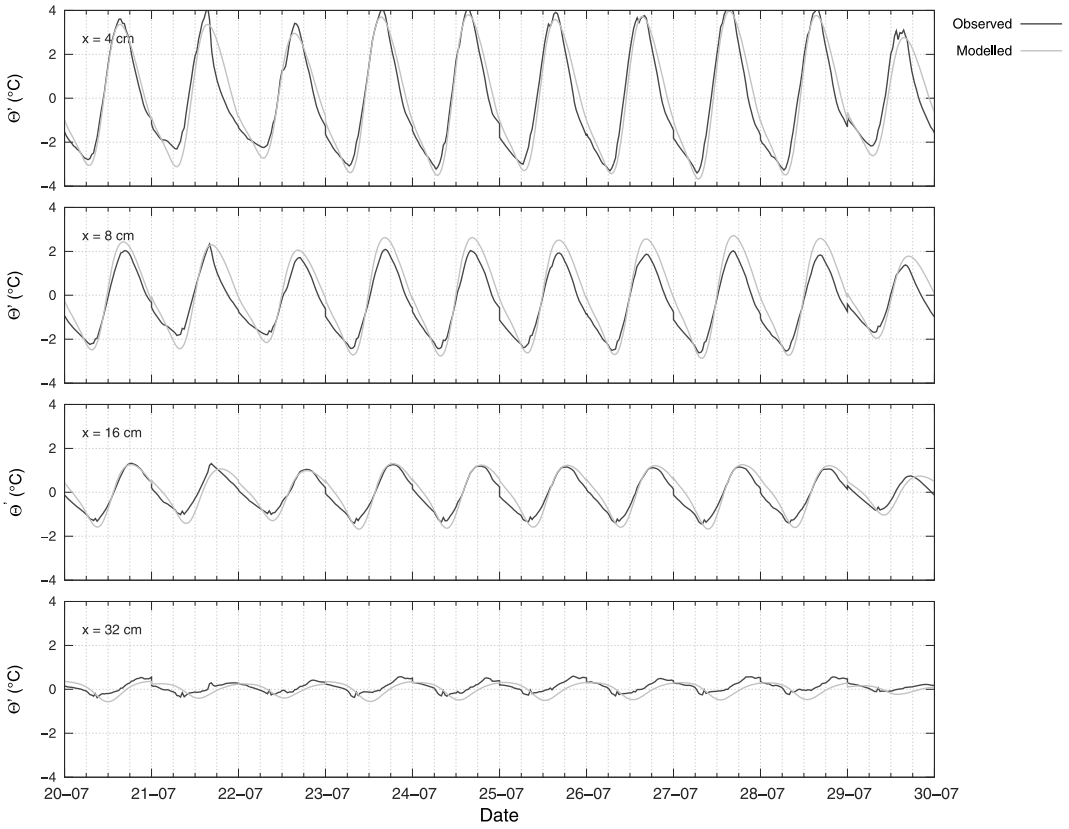

Figure 10. Observed and reconstructed soil temperature fluctuations at the depths of 4, 8, 16, and 32 cm, during 10 consecutive days (July 1997, model application). Data collected by the NOAA/ATDD micrometeorological station at Chickasha (Little Washita watershed, Oklahoma, USA) [*Meyers*, 2015].

Anyway, if the performance of the model is assessed on the basis of the plotted time series, it is observed that it is able to accurately reproduce the temperature signals. As an example, in fact, the weighting factors reported in Table 2 were used to approximate the daily soil temperature fluctuations and the soil heat flux both for four consecutive clear-sky days chosen in the calibration period (Figure 7) and for the 10 consecutive rainy and clear-sky days chosen in 2014 (Figure 8). The soil heat fluxes, which are presented in the figures, were computed by means of equation (16) coupled with equation (B2), once estimated the soil thermal conductivity according to the fitted Kersten relationship (23). The model proves to be very effective at reconstructing both the minima, the maxima, and the dynamics of the temperature series in both the test periods, with a small phase delay in 2014. Even if it is meaningfully sensitive to the estimate of the thermal conductivity, the model proves to be also effective at reproducing the maxima and the dynamics of the soil heat flux with a slight overestimation of the magnitude of the minima. The midnight discontinuities in the soil temperature fluctuations, which are evident in Figure 8 and in the following Figures 9 and 10, are a consequence of the unsteadiness of the daily average soil temperature.

4.1. Example of Application to a Different Site

In order to demonstrate the applicability of our procedure in a different environment, we selected some days of soil temperature data measured at the NOAA/Atmospheric Turbulence and Diffusion Division (ATDD) micrometeorological station sited near Chickasha, within the Little Washita watershed, Oklahoma (USA). The station was designed for long-term flux monitoring and started operating in 1996. In 1997 it was involved in the meteorological network of the SGP97 research project [*Jackson*, 1997; *Famiglietti et al.*, 1999], and collected data until 1999. The station was placed in a pasture over a gently rolling terrain surrounded by flat and homogeneous topography. The upper 60 cm of soil are clay loam with estimated bulk density of 1.6 g cm^{-3}. Half-hourly soil temperature series are available at the depths of 2, 4, 8, 16, 32, and 64 cm [*Meyers*, 2015]. Temperature data collected during two series of 10 consecutive days (from 29 June to 9 July 1997 and from 20 July to 30 July 1997), were selected and items 1 to 4 of the procedure applied. In Figures 9 and 10 the obtained

soil temperature fluctuations are presented and compared with the observations. Series corresponding to the depths of 4, 8, 16, and 32 cm were selected because they were deep enough to assume that the conduction was the main heat transfer process and the assumption of linearity of the average temperature profile $\overline{\Theta}(x)$ was adhered to. The modeled temperatures are in good agreement with the exception of 4 July 1997 (Figure 9), when the temperature series, due to a rainfall event, did not show the typical pattern of dry days. The obtained results therefore support the idea that the $\mathcal{F}_n$ coefficients are site independent and our procedure is of general applicability.

5. Conclusions

Based on the observation that the temperature of the upper soil layers shows during dry days, a typical asymmetric periodic-like pattern, an analytical solution of the Fourier equation, expressed in terms of trigonometric series, was parametrized in order to accurately reconstruct the soil thermal dynamics. As it was recognized that, below the surface, the pattern of the temperature measurements does not depend on the soil thermal properties, a set of weighting coefficients (13) only depending on the surface temperature shape and phase was evidenced in the analytical solution. The proposed coefficients characterize the amplitude ($\epsilon_{A,n}$), the damping depth ($\epsilon_{D,n}$), and the phase ($\phi_{o,n}$) of each harmonic. On the basis of the data collected during the CividatEX Experiment (2012–2014), in Italy, the weighting coefficients were determined and presented in Table 2. By means of the proposed coefficients the soil temperature field can be accurately reconstructed once known the actual measured amplitude and the bulk damping depth of the temperature profiles. Therefore, the method applies once at least two temperature series at different depth are known or it is known only one series and the soil thermal diffusivity.

The method allowed to describe the temperature field of the investigated site with good results as it is reported in Figures 7 and 8 both for the calibration and for the validation periods. Even if it was developed and calibrated in dry days, the method was effective to reconstruct the temperature series also during some rainy days. Moreover, it was observed that, in agreement with the theory, the asymmetry of the patterns of the temperature series is described by higher-order harmonics (Figure 6), but good results are obtained even by means of two harmonics only.

In view of estimating the soil heat flux, either the thermal conductivity or the soil thermal capacity should be known or empirically determined on the basis of experimental data. In our case the application of Kersten's method [*Kersten*, 1949] provided a realistic approach to estimate the thermal conductivity after measured heat fluxes. As shown in the last row of Figures 7 and 8, the method proved to be effective also at reconstructing the soil heat flux both in calibration and in validation periods.

Finally, in order to test the portability of the procedure and of the calibrated coefficients $\mathcal{F}_n$ also in different environments, we reconstructed the temperature series recorded at various depths during two series of 10 consecutive days in 1997, by the NOAA/ATDD micrometeorological station at Chickasha (Oklahoma, USA). The procedure proved to be effective at reconstructing the temperature measurements with a good agreement, thus supporting the idea that the $\mathcal{F}_n$ coefficients are site independent and that the procedure is of general applicability.

Appendix A: Fourier Decomposition of Temperature Profiles

The temperature field is rewritten as the sum of a constant term and of a fluctuating one as in equation (2) which is here recalled:

$$\Theta(x,t) = \overline{\Theta}(x) + \Theta'(x,t). \tag{A1}$$

Assuming that the average temperature field $\overline{\Theta}(x)$ is either uniform or, as a first approximation, linear in the upper soil (and we remark that it is in this case a solution of the Fourier equation), the daily average temperature profile $\overline{\Theta}(x)$ is interpolated by

$$\overline{\Theta}(x) = \overline{\Theta}_o - \Gamma_{\overline{\Theta}} x. \tag{A2}$$

In equation (A2) $\overline{\Theta}_o = \overline{\Theta}(0)$ represents the daily average temperature at the soil surface and $\Gamma_{\overline{\Theta}} = -\frac{\partial \overline{\Theta}}{\partial x}$ represents the vertical gradient of the daily average temperature.

If we assume that the temperature fluctuation is a periodic function with a daily period, $\Theta'(x,t)$ can be represented by means of a discrete trigonometric Fourier series:

$$\Theta'(x,t) = \sum_{n=1}^{\infty} \left[a_{x,n} \cos(n\omega t) + b_{x,n} \sin(n\omega t) \right], \tag{A3}$$

where n is the order of the harmonic; $\omega = \frac{2\pi}{T}$ is the daily radial frequency, with $T = 86,400$ s; and $a_{x,n}$ and $b_{x,n}$ are the Fourier coefficients computed for the measured temperature signal at the depth x. The Fourier coefficients $a_{x,n}$ and $b_{x,n}$ are defined by

$$a_{x,n} = \frac{\omega}{\pi} \int_0^T \Theta'(x,\tau) \cos(n\omega\tau)\, \mathrm{d}\tau, \tag{A4}$$

$$b_{x,n} = \frac{\omega}{\pi} \int_0^T \Theta'(x,\tau) \sin(n\omega\tau)\, \mathrm{d}\tau. \tag{A5}$$

According to (2), as a Dirichlet boundary condition the surface soil temperature is given in the form:

$$\Theta_o(t) = \overline{\Theta}_o + \Theta'_o(t), \tag{A6}$$

where $\Theta_o(t) = \Theta(0,t)$ is the instantaneous soil temperature, $\overline{\Theta}_o = \overline{\Theta}(0)$ is the daily average temperature, and $\Theta'_o(t) = \Theta'(0,t)$ is the fluctuating component, all referred at the soil surface ($x = 0$). By means of (A3)–(A5), equation (A6) is rewritten in the form

$$\Theta_o(t) = \overline{\Theta}_o + \sum_{n=1}^{\infty} \left[a_{o,n} \cos(n\omega t) + b_{o,n} \sin(n\omega t) \right], \tag{A7}$$

where $a_{o,n}$ and $b_{o,n}$ are the Fourier coefficients of the fluctuating component $\Theta'_o(t)$ observed at the surface. The second boundary condition is obtained with the usual constraint that $\Theta'(x,t)$ is limited at increasing x.

Under these assumptions a classical solution of the problem is given in terms of stabilized periodic functions with the same periodicity of the upper boundary condition. The solution is given in the form of equation (3) which is here recalled:

$$\Theta(x,t) = \overline{\Theta}(x) + \sum_{n=1}^{\infty} {}^{A}\Theta_{x,n} \sin\left(n\omega t + \phi_n(x)\right). \tag{A8}$$

The amplitude ${}^{A}\Theta_{x,n}$ and the phase $\phi_n(x)$ of the nth harmonic are related to the Fourier coefficients according to the relationships:

$${}^{A}\Theta_{x,n} = \sqrt{a_{x,n}^2 + b_{x,n}^2}, \tag{A9}$$

$$\phi_n(x) = \arctan\left(\frac{a_{x,n}}{b_{x,n}}\right). \tag{A10}$$

Appendix B: Heat Flux and Soil Stored Heat

Once obtained the temperature profiles (3), both the soil heat flux $H(x,t)$ $\left[\mathrm{MT}^{-3}\right]$ at a certain depth, the heat $S^{[x_1;x_2]}(t)$ $\left[\mathrm{MT}^{-2}\right]$ stored in a soil layer of thickness $x_2 - x_1$ and its rate of change $\frac{\partial S^{[x_1;x_2]}}{\partial t}$ $\left[\mathrm{MT}^{-3}\right]$ can be analytically computed. All the previous quantities are intended to be defined per unitary surface. According to the Fourier law, the soil heat flux is

$$H(x,t) = -k_T \frac{\partial \Theta}{\partial x} \tag{B1}$$

$$= -k_T \left[\frac{\partial \overline{\Theta}}{\partial x} + \frac{\partial \Theta'}{\partial x} \right], \tag{B2}$$

where k_T $\left[\mathrm{MLT}^{-3}\Theta^{-1}\right]$ is the soil thermal conductivity. Accounting for (3), with ${}^{A}\Theta_{x,n}$ and $\phi_n(x)$ given by (A9) and (A10), $H(x,t)$ takes the form

$$H(x,t) = -k_T\left[\frac{\partial\overline{\Theta}}{\partial x} - \sqrt{2}\sum_{n=1}^{\infty}\frac{{}^{A}\Theta_{o,n}}{D_n}\mathrm{e}^{-\frac{x}{D_n}}\sin\left(n\omega t + \phi_n(x) + \frac{\pi}{4}\right)\right], \tag{B3}$$

and the heat flux at the soil surface is given by

$$H(0,t) = -k_T\left[\frac{\partial\overline{\Theta}}{\partial x} - \sqrt{2}\sum_{n=1}^{\infty}\frac{{}^{A}\Theta_{o,n}}{D_n}\sin\left(n\omega t + \phi_{o,n} + \frac{\pi}{4}\right)\right]. \tag{B4}$$

Let us define the stored heat as

$$S^{[x_1;x_2]}(t) = \int_{x_1}^{x_2} c_T\,\Theta(\xi,t)\mathrm{d}\xi, \tag{B5}$$

where c_T $\left[\mathrm{ML}^{-1}\mathrm{T}^{-2}\Theta^{-1}\right]$ is the volumetric soil thermal capacity, linked to the soil thermal conductivity and to the soil thermal diffusivity by means of the relationship:

$$k_T = \alpha c_T. \tag{B6}$$

The rate of change $\frac{\partial S^{[x_1;x_2]}}{\partial t}$ is given by

$$\frac{\partial S^{[x_1;x_2]}}{\partial t} = \int_{x_1}^{x_2} c_T\frac{\partial\Theta}{\partial t}\mathrm{d}\xi \equiv \int_{x_1}^{x_2} c_T\frac{\partial\Theta'}{\partial t}\mathrm{d}\xi, \tag{B7}$$

thus obtaining, after a repeated integration by parts

$$\frac{\partial S^{[x_1;x_2]}}{\partial t} = -c_T\frac{\omega}{\sqrt{2}}\sum_{n=1}^{\infty} nD_n\,{}^{A}\Theta_{o,n}\left[\mathrm{e}^{-\frac{\xi}{D_n}}\sin\left(n\omega t + \phi_n(\xi) + \frac{\pi}{4}\right)\right]_{x_1}^{x_2}. \tag{B8}$$

In (B8) the term in square brackets is computed between the two depths x_2 and x_1. When $x_1 = 0$ and $x_2 = x$ equation (B8) becomes

$$\frac{\partial S^{[0;x]}}{\partial t} = c_T\frac{\omega}{\sqrt{2}}\sum_{n=1}^{\infty} nD_n\,{}^{A}\Theta_{o,n}\left[\sin\left(n\omega t + \phi_{o,n} + \frac{\pi}{4}\right) - \mathrm{e}^{-\frac{x}{D_n}}\sin\left(n\omega t + \phi_n(x) + \frac{\pi}{4}\right)\right]. \tag{B9}$$

Acknowledgments

Part of the research was funded in the framework of the research project PRIN 2008*"Valutazione delle risorse idriche e loro gestione in scenari di cambiamento climatico"* coordinated by Goffredo La Loggia, which is acknowledged. Data from research project SGP97 Surface are provided by NCAR/EOL under sponsorship of the National Science Foundation (http://data.eol.ucar.edu). This research was part of the research activity of the Doctorate in "Natural Risks Assessment and Management" of the first author at the Università degli Studi di Brescia. The Doctorate program coordinator Baldassare Bacchi is kindly acknowledged. The Editor Giovanni Coco, the Associate Editor, the reviewer Zhihua Wang, and two anonymous reviewers are kindly acknowledged for their valuable comments and suggestions. Data used in this study can be consulted by contacting the scientific responsible of the meteorological station Roberto Ranzi.

References

Ballard, T. M. (1972), Subalpine soil temperature regimes in southwestern British Columbia, *Arct. Alpine Res.*, *4*(2), 139–146.

Bandini, A., (1931), Tipi pluviometrici dominanti sulle regioni italiane, Tech. Rep., Ministero dei Lavori Pubblici, Roma, Italy.

Barr, A. G., G. van der Kamp, T. A. Black, J. H. McCaughey, and Z. Nesic (2012), Energy balance closure at the BERMS flux towers in relation to the water balance of the White Gull Creek watershed 1999–2009, , Land–Atmosphere Interactions: Advances in Measurement, Analysis, and Modeling – A Tribute to T. Andrew Black,, *Agric. Forest Meteorol.*, *153*, 3–13, doi:10.1016/j.agrformet.2011.05.017.

Brutsaert, W. (1982), *Evaporation Into the Atmosphere: Theory, History, and Applications*, 299 pp., Reidel; Sold and distributed in the U.S.A. and Canada by Kluwer Boston Dordrecht, Holland; Boston, Hingham, Mass.

Carslaw, H. S., and J. C. Jaeger (1959), *Conduction of Heat in Solids*, 2 ed., Oxford Sci. Publ., Clarendon Press, New York.

Ca'Zorzi, F., and G. Dalla Fontana (1986), Improved utilization of maximum and minimum daily temperature in snowmelt modelling, in *Modelling Snowmelt-Induced Processes*, pp. 141–150, (Proceedings of the Budapest Symposium, July 1986), IAHS Publication n. 155, Budapest, Hungary.

Chen, S. (2008), Thermal conductivity of sands, *Heat Mass Transfer*, *44*(10), 1241–1246, doi:10.1007/s00231-007-0357-1.

Chudnovskii, A. F. (1962), *Heat Transfer in the Soil*, Trans. en. IPST staff, Israel Program for Scientific Translations Ltr., Jerusalem. (Original ed. Fizika teploobmena v pochve, OGIZ State publishing house of technical–theoretical literature Leningrad–Moscow, 1948).

Cosenza, P., R. Guérin, and A. Tabbagh (2003), Relationship between thermal conductivity and water content of soils using numerical modelling, *Eur. J. Soil Sci.*, *54*(3), 581–588, doi:10.1046/j.1365-2389.2003.00539.x.

Coughlan, M., and R. Avissar (1996), The Global Energy and Water Cycle Experiment (GEWEX) Continental-Scale International Project (GCIP): An overview, *J. Geophys. Res.*, *101*(D3), 7139–7147, doi:10.1029/96JD00125.

Crank, J. (1979), *The Mathematics of Diffusion*, 2 ed., Oxford Univ. Press, Clarendon Press, Oxford, U. K.

Endrizzi, S., S. Gruber, M. Dall'Amico, and R. Rigon (2014), GEOtop 2.0: Simulating the combined energy and water balance at and below the land surface accounting for soil freezing, snow cover and terrain effects, *Geosci. Model Dev.*, *7*(6), 2831–2857, doi:10.5194/gmd-7-2831-2014.

Evett, S. R., N. Agam, W. P. Kustas, P. D. Colaizzi, and R. C. Schwartz (2012), Soil profile method for soil thermal diffusivity, conductivity and heat flux: Comparison to soil heat flux plates, the Bushland Evapotranspiration and Agricultural Remote Sensing Experiment 2008, *Adv. Water Resour.*, *50*, 41–54, doi:10.1016/j.advwatres.2012.04.012.

Falocchi, M., A. Negm, S. Barontini, and R. Ranzi, (2015), The CividatEX Experiment: I. Setup and collected data (July 2012–December 2014), Tech. Rep., Univ. degli Studi di Brescia – DICATAM, Brescia, Italy.

Famiglietti, J. S., J. A. Devereaux, C. A. Laymon, T. Tsegaye, P. R. Houser, T. J. Jackson, S. T. Graham, M. Rodell, and P. J. van Oevelen (1999), Ground-based investigation of soil moisture variability within remote sensing footprints during the Southern Great Plains 1997 (SGP97) Hydrology Experiment, *Water Resour. Res.*, *35*(6), 1839–1851, doi:10.1029/1999WR900047.

Farouki, O. T. (1981), *Thermal Properties of Soils*, Cold Regions Research and Engineering Laboratory Report 82-8, U.S. Army Corps of Engineers, Hanover, N. J.

Foken, T. (2008), The energy balance closure problem: An overview, *Ecol. Appl.*, *18*(6), 1351–1367, doi:10.1890/06-0922.1.

Gao, Z., X. Fan, and L. Bian (2003), An analytical solution to one-dimensional thermal conduction-convection in soil, *Soil Sci.*, *168*(2), 99–107.

Gao, Z., D. H. Lenschow, R. Horton, M. Zhou, L. Wang, and J. Wen (2008), Comparison of two soil temperature algorithms for a bare ground site on the Loess Plateau in China, *J. Geophys. Res.*, *113*, D18105, doi:10.1029/2008JD010285.

Heusinkveld, B. G., A. F. G. Jacobs, A. A. M. Holtslag, and S. M. Berkowicz (2004), Surface energy balance closure in an arid region: Role of soil heat flux, *Agric. Forest Meteorol.*, *122*(1–2), 21–37, doi:10.1016/j.agrformet.2003.09.005.

Huang, F., W. Zhan, W. Ju, and Z. Wang (2014), Improved reconstruction of soil thermal field using two-depth measurements of soil temperature, *J. Hydrol.*, *519, Part A*, 711–719, doi:10.1016/j.jhydrol.2014.08.014.

Jackson, T. J. (1997), Southern Great Plains 1997 (SGP97) Hydrology Experiment Plan. [Available at http://hydrolab.arsusda.gov/sgp97/, Accessed: 23 June 2015.]

Jacobs, A. F. G., B. G. Heusinkveld, and A. A. M. Holtslag (2011), Long-term record and analysis of soil temperatures and soil heat fluxes in a grassland area, the Netherlands, *Agric. Forest Meteorol.*, *151*(7), 774–780, doi:10.1016/j.agrformet.2011.01.002.

Jaynes, D. B. (1990), Temperature variations effect on field-measured infiltration, *Soil Sci. Soc. Am. J.*, *54*(2), 305–312, doi:10.2136/sssaj1990.03615995005400020002x.

Johansen, O. (1975), Thermal conductivity of soils, PhD thesis, Univ. of Trondheim, Norway. CRREL Draft Translation 637, July 1977, ADA 044002.

Kersten, M. S. (1949), *Laboratory Research for the Determination of the Thermal Properties of Soils*, Research Laboratory Eng., Univ. Minnesota, Minnesota.

Khydyakov, O. I., and O. V. Reshotkin (2014), Temperature dynamics in sandy and loamy forest-tundra soils of the Polar Urals in relation to climate change, *Eurasian Soil Sci.*, *47*(12), 1245–1258, doi:10.1134/S1064229314120060.

Kiehl, J. T., and K. E. Trenberth (1997), Earth's annual global mean energy budget, *Bull. Am. Meteorol. Soc.*, *78*(2), 197–208.

Liang, X., D. P. Lettenmaier, E. F. Wood, and S. J. Burges (1994), A simple hydrologically based model of land surface water and energy fluxes for general circulation models, *J. Geophys. Res.*, *99*(D7), 14,415–14,428, doi:10.1029/94JD00483.

Liu, F., F. Tao, S. Li, S. Zhang, D. Xiao, and M. Wang (2014), Energy partitioning and environmental influence factors in different vegetation types in the GEWEX Asian Monsoon Experiment, *Frontiers Earth Sci.*, *8*(4), 582–594, doi:10.1007/s11707-014-0429-8.

Meyers, T. (2015), SGP97 Surface: NOAA/ATDD Little Washita. [Available at http://data.eol.ucar.edu/codiac/ dss/id=25.015, Accessed: 23 June 2015.]

Mogensen, V. O. (1970), The calibration factor of heat flux meters in relation to the thermal conductivity of the surrounding medium, *Agric. Meteorol.*, *7*, 401–410, doi:10.1016/0002-1571(70)90035-X.

Murphy, D. M., S. Solomon, R. W. Portmann, K. H. Rosenlof, P. M. Forster, and T. Wong (2009), An observationally based energy balance for the Earth since 1950, *J. Geophys. Res.*, *114*, D17107, doi:10.1029/2009JD012105.

Negm, A., M. Falocchi, S. Barontini, B. Bacchi, and R. Ranzi (2013), Assessment of the water balance in an alpine climate: Setup of a micrometeorological station and preliminary results, Four Decades of Progress in Monitoring and Modeling of Processes in the Soil–Plant–Atmosphere System: Applications and Challenges, *Proc. Environ. Sci.*, *19*, 275–284, doi:10.1016/j.proenv.2013.06.032.

Ochsner, T. E., T. J. Sauer, and R. Horton (2007), Soil heat storage measurements in energy balance studies, *Agron. J.*, *99*(1), 311–319, doi:10.2134/agronj2005.0103S.

Philip, J. R. (1957), Evaporation, and moisture and heat fields in the soil, *J. Meteorol.*, *14*, 354–366, doi:10.1175/1520–0469(1957)014<0354:EAMAHF>2.0.CO;2.

Philip, J. R. (1961), The theory of heat flux meters, *J. Geophys. Res.*, *66*(2), 571–579, doi:10.1029/JZ066i002p00571.

Philip, J. R., and D. A. De Vries (1957), Moisture movement in porous materials under temperature gradients, *Eos Trans. AGU*, *38*(2), 222–232, doi:10.1029/TR038i002p00222.

Pilotti, M., S. Succi, and G. Menduni (2002), Energy dissipation and permeability in porous media, *Europhys. Lett.*, *60*, 72–78, doi:10.1209/epl/i2002-00320-5.

Ranzi, R., G. Grossi, A. Gitti, and S. Taschner (2010), Energy and mass balance of the Mandrone Glacier (Adamello, Central Alps), *Geografia Fisica e Dinamica Quaternaria*, *33*(1), 45–60.

Sauer, T. J., and R. Horton (2005), Soil heat flux, in *Micrometeorology in Agricultural Systems, Agron. Monogr.,* No. 47, edited by J. L. Hatfield and J. M. Baker, pp. 131–154, Am. Soc. Agron., Madison, Wis.

Sauer, T. J., T. E. Ochsner, J. L. Heitman, R. Horton, B. D. Tanner, O. D. Akinyemi, G. Hernandez Ramirez, and T. B. Moorman (2008), Careful measurements and energy balance closure—The case of soil heat flux, *paper presented at 28th Conference on Agricultural and Forest Meteorol*, American Meteorological Society (AMS) Committee on Agricultural and Forest Meteorology, Orlando, Fla, 28 April–2 May.

Taschner, S., and R. Ranzi (2002), Comparing the opportunities of Landsat-TM and Aster data for monitoring a debris covered glacier in the Italian Alps within the GLIMS project, in *IEEE International on Geoscience and Remote Sensing Symposium (IGARSS '02)*, vol. 2, pp. 1044–1046, IEEE, Toronto, Canada.

Trenberth, K. E., J. T. Fasullo, and J. Kiehl (2009), Earth's global energy budget, *Bull. Am. Meteorol. Soc.*, *90*(3), 311–323.

U.S. Department of Agriculture (1999), *Soil Taxonomy: A Basic System of Soil Classification for Making and Interpreting Soil Surveys*, 2nd ed., Natural Resour. Conservation Service. U.S. Department of Agric., Agric. Handbook 436, U.S. Gov. Print Off., Washington, D. C.

van Wijk, W. R., and D. A. De Vries (1963), Periodic temperature variations in a homogeneous soil, in *Physics of Plant Environment*, edited by W. R. van Wijk, chap. 4, pp. 102–143, North-Holland Publ. Comp., Amsterdam.

Wang, J., and R. L. Bras (1999), Ground heat flux estimated from surface soil temperature, *J. Hydrol.*, *216*(3-4), 214–226, doi:10.1016/S0022-1694(99)00008-6.

Wang, L., Z. Gao, R. Horton, D. H. Lenschow, K. Meng, and D. B. Jaynes (2012), An analytical solution to the one-dimensional heat conduction-convection equation in soil, *Soil Sci. Soc. Am. J.*, *76*(6), 1978–1986, doi:10.2136/sssaj2012.0023N.

Wang, Z.-H. (2012), Reconstruction of soil thermal field from a single depth measurement, *J. Hydrol.*, *464-465*, 541–549, doi:10.1016/j.jhydrol.2012.07.047.

Wang, Z.-H., and E. Bou-Zeid (2012), A novel approach for the estimation of soil ground heat flux, *Agric. Forest Meteorol.*, *154-155*, 214–221, doi:10.1016/j.agrformet.2011.12.001.

Wang, Z.-H., E. Bou-Zeid, and J. A. Smith (2011), A spatially-analytical scheme for surface temperatures and conductive heat fluxes in urban canopy models, *Boundary Layer Meteorol.*, *138*(2), 171–193, doi:10.1007/s10546-010-9552-6.

Weber, S., A. Graf, and B. G. Heusinkveld (2007), Accuracy of soil heat flux plate measurements in coarse substrates—Field measurements versus a laboratory test, *Theor. Appl. Climatol.*, *89*(1-2), 109–114, doi:10.1007/s00704-006-0256-2.

Wild, M., D. Folini, M. Z. Hakuba, C. Schär, S. I. Seneviratne, S. Kato, D. Rutan, C. Ammann, E. F. Wood, and G. König-Langlo (2014), The energy balance over land and oceans: An assessment based on direct observations and CMIP5 climate models, *Clim. Dyn.*, *44*, 3393–3429, doi:10.1007/s00382-014-2430-z.

Wilson, K., et al. (2002), Energy balance closure at FLUXNET sites, FLUXNET 2000 Synthesis, *Agric. Forest Meteorol.*, *113*(1–4), 223–243, doi:10.1016/S0168-1923(02)00109-0.